Identifying the Dirac point composition in Bi, Sb, alloys using the temperature dependence of quantum oscillations



Special Collection: Engineering and Understanding of Thermal Conduction Materials

Joon Sang Kang ➡; Dung Vu ⑩; Joseph P. Heremans ⑩



J. Appl. Phys. 130, 225106 (2021) https://doi.org/10.1063/5.0068312

A CHORUS





Articles You May Be Interested In

Study of the Shubnikov–de Haas effect in $Bi_{1-X}Sb_X$ semimetallic alloys

Sov. J. Low Temp. Phys. (January 1978)

Topological features of quantum transport in $bi_{1-x}Sb_x$ ($0 \le x \le 0.2$) bicrystals

Low Temp. Phys. (January 2023)

Electronic transport properties of Pb(Bi_{1-x}Sb_x) ₂(Te_{1-v}Se_v) ₄ topological insulator

J. Appl. Phys. (May 2022)





22 January 2025 20:01:36





Identifying the Dirac point composition in $Bi_{1-x}Sb_x$ alloys using the temperature dependence of quantum oscillations

Cite as: J. Appl. Phys. 130, 225106 (2021); doi: 10.1063/5.0068312 Submitted: 24 August 2021 · Accepted: 18 November 2021 · Published Online: 9 December 2021







Joon Sang Kang,^{1,a)} Dung Vu,¹ 🔟 and Joseph P. Heremans^{1,2,3} 📵



AFFILIATIONS

- ¹Department of Mechanical and Aerospace Engineering, The Ohio State University, Columbus, Ohio 43210, USA
- ²Department of Physics, The Ohio State University, Columbus, Ohio 43210, USA
- ³Department of Materials Science and Engineering, The Ohio State University, Columbus, Ohio 43210, USA

Note: This paper is part of the Special Topic on Engineering and Understanding of Thermal Conduction in Materials.

a)Author to whom correspondence should be addressed: kang.1284@osu.edu

ABSTRACT

The thermal chiral anomaly is a new mechanism for thermal transport that occurs in Weyl semimetals (WSMs). It is attributed to the gen- 🞖 eration and annihilation of energy at Weyl points of opposite chirality. The effect was observed in the Bi_{1-x}Sb_x alloy system, at x = 11% and $\frac{8}{3}$ 15%, which are topological insulators at zero field and driven into an ideal WSM phase by an external field. Given that the experimental uncertainty on x is of the order of 1%, any systematic study of the effect over a wider range of x requires precise knowledge of the transition $\frac{8}{5}$ composition x_c at which the electronic bands at the L-point in these alloys have Dirac-like dispersions. At $x > x_c$ the L-point bands are inverted and become topologically non-trivial. In the presence of a magnetic field along the trigonal direction, these alloys become WSMs. This paper describes how the temperature dependence of the frequency of the Shubnikov-de Haas oscillations F(x,T) at temperatures of the order of the cyclotron energy can be used to find x_c and characterize the topology of the electronic Fermi surface. Semimetallic Bi_{1-x}Sb_x alloys with topologically trivial bands have $dF(x,T)/dT \ge 0$; those with Dirac/Weyl fermions display dF(x,T)/dT < 0.

Published under an exclusive license by AIP Publishing. https://doi.org/10.1063/5.0068312

INTRODUCTION

Weyl semimetals (WSMs) are characterized by an electronic band structure, which has linearly dispersing bands that intersect at Weyl points (WPs) in a system that breaks time reversal symmetry (TRS) or inversion symmetry (IS). The WPs come in pairs located at specific points in the k-space, $+\mathbf{k}_0$ and $-\mathbf{k}_0$, which are the source and sink of Berry curvatures. The dispersion relation near the WPs is characteristic of massless particles and 3-dimensional,

$$E(\mathbf{k}) = \pm v_F \hbar \mathbf{k}, \quad \mathbf{k} = (k_x, k_y, k_z). \tag{1}$$

Here, v_F is the Fermi velocity, \hbar is Planck's constant, and \mathbf{k} is measured relative to $\pm \mathbf{k}_0$ for the respective WP in the pair. The electrical and thermal transport properties of WSM display the chiral anomaly. First predicted by Nielsen and Ninomiya, the chiral anomaly manifests itself as an extra electrical conductivity that appears in the samples in the presence of parallel electric (E) and magnetic (B) fields applied in the direction of the WP separation in the k-space, i.e., the direction from $-\mathbf{k}_0$ to $+\mathbf{k}_0$. In the extreme quantum limit (EQL), when all electrons and holes are on the last Landau level, this additional electrical conductivity is given by

$$\sigma_{zz}(B_z) = N_w \frac{e^3 v \tau}{4\pi^2 \hbar^2} B_z, \tag{2}$$

where N_w is the number of degenerate pairs of WPs in the Brillouin zone, e is the electron charge, v is the electron velocity, and τ is the inter-Weyl point scattering time. The thermal chiral anomaly² manifests itself as the creation of an additional electronic thermal conductivity that appears in the samples in the presence of parallel thermal gradient (∇T) and **B** applied in the direction of the WP separation in the k-space. In the extreme quantum limit, it is

given by²

$$\kappa_{zz}(B_z) = N_w T \frac{\pi^2}{3} \frac{k_B^2 e v \tau}{4\pi^2 \hbar^2} B_z, \tag{3}$$

where T is the temperature and k_B is the Boltzmann constant. The additional electrical conduction manifests itself in WSMs as a negative longitudinal magnetoresistance (NLMR). Unfortunately, observing an NLMR is not a sufficient proof of the existence of the anomaly because extrinsic effects caused by the applied magnetic field on the current distribution in the sample, most notably current-jetting effects,3,4 also give rise to an NMLR. The additional thermal conductivity is observed as a positive longitudinal thermal conductivity,2 which is a more reliable indicator of the existence of the anomaly because no electrical current flows during thermal conductivity measurements and because the lattice thermal conductivity evens out the heat distribution lines and is insensitive to field. In Ref. 2, the increase in both electrical and thermal conductivity was observed in high magnetic fields applied along the trigonal (z) direction in $Bi_{1-x}Sb_x$ alloys with $x = 10.5 \pm 0.5$ at. % and 15.1 ± 0.7 at. % (referred to nominally 11% and 15%).

The evolution of the band extrema in $Bi_{1-x}Sb_x$ alloys as a function of x at zero field is shown schematically in Fig. 1(a).⁵ In topologically trivial semiconductors or semimetals, the states with a symmetric wavefunction (here denoted s) constitute the conduction band, whereas the valence band consists of states with an antisymmetric (here denoted a) wavefunction. This is the case in $Bi_{1-x}Sb_x$ alloys for $x < x_c$. With increasing Sb content, the gap E_g between

the L_s and L_a bands closes until it reaches zero at a concentration $x_c \approx 5 \pm 1$ at. %). The green line in Fig. 1(a) represents the minimum of a second valence band at the T-point of the Brillouin zone. Holes in that band have conventional parabolic dispersions and, at any value of x, are topologically trivial. For $x > x_c$, the bands are inverted: the conduction band has a symmetry (denoted L_a) and the valence band has s symmetry (denoted L_s). At x > 8% or 9%, the T-hole-band maximum falls below the L_s valence band, and the alloys become direct-gap topological insulators, in fact, the first topological insulators identified experimentally by ARPES measurements.⁶ At zero field, the 11% and 15% alloys are directgap semiconductors with gaps ($E_g \approx 13 \text{ meV}$ at x = 11% and $E_g \approx 30 \text{ meV}$ at x = 15%) at the L-points of the Brillouin zone. In the presence of a strong magnetic field oriented along the trigonal z-axis, their bandgap closes with increasing field because of the extremely large Landé g-factor in these alloys. Above a critical applied magnetic field B_z , the x = 11% and 15% alloys form ideal WSMs, meaning that the dispersions are given by Eq. (1), and the electrochemical potential μ is at the WP energy ($\mu = 0$) within the experimental energy range. The WPs are centered around the L-points of the Brillouin zone and separated along a direction that is mostly aligned with the trigonal z-axis so that $\kappa_{zz}(B_z)$ shows a strong thermal chiral anomaly, which gives rise to a very large increase in electronic thermal conductivity in the magnetic field.² There are also no trivial bands at energy μ and no unintentional doping. Thus, μ is pinned to the WPs because those points have the minimum system density of states (DOS); an ideal WSM displays no Shubnikov-de Haas (SdH) oscillations. The Fermi surface 83

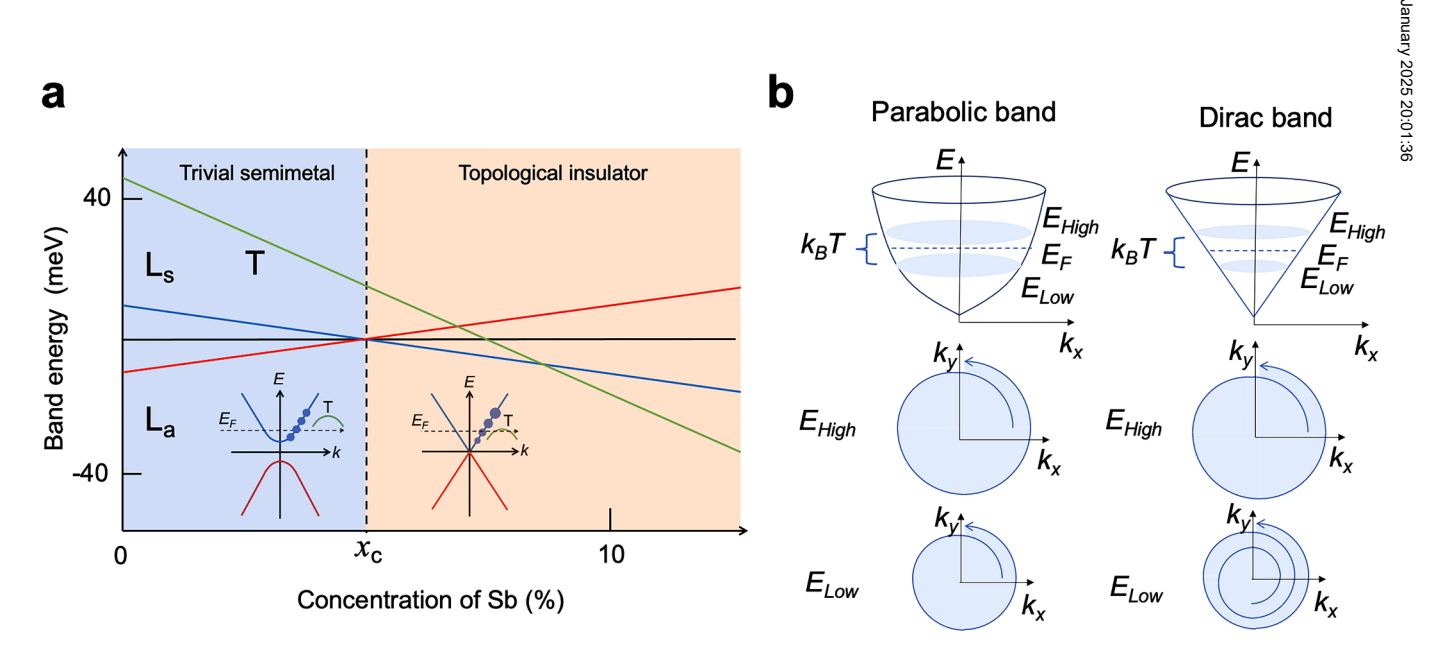


FIG. 1. (a) Evolution of the band structure of $\text{Bi}_{1-x}\text{Sb}_x$ alloys as a function of antimony concentration x (in at. %). The insets show the dispersion relation in the topologically trivial phase ($x < x_c$) and at the composition x_c at which the L-point bands have a Dirac dispersion. $x_c \approx 5 \pm 1$ at. %. The blue dots schematically show the magnitude of effective mass of carriers distributed over $k_B T$ around $E_F = \mu(T = 0)$; it does not change in a parabolic band but decreases with energy in a Dirac band. This gives rise to a change in the frequency of the quantum oscillations with temperature. (b) Schematic of a physical origin of a temperature-dependent SdH oscillation frequency change. Heavier, higher-energy charge carriers are less likely to complete cyclotron orbits before encountering a phonon that perturbs the phase coherence of their wavefunction.

While the experiments in Ref. 2 were carried out on ideal WSMs, only alloys with 9% < x < 18% are expected to fall in that category. Above about $x \approx 18\%$, a new trivial valence band, the H-band, crosses the L_s band, making the alloys indirect-gap semiconductors at zero field, and above $x \approx 22\%$, it crosses the L_a band, making the alloys antimony-like semimetals.4 In order to extend the thermal chiral anomaly to room temperature, it is necessary to investigate $Bi_{1-x}Sb_x$ alloys with as wide range of x as possible because Bi_{1-x}Sb_x is expected to give rise to a WSM phase in the magnetic field as a function of x, even if those WSMs are not ideal. This means μ in them falls in a band and not at the WPs and if their Fermi surfaces contain trivial pockets. Weyl physics is expected to remain even if μ falls inside but within the bandwidth of the Weyl bands. Here, we focus our work on alloys in the 0% < x < 7% range.

Note that the experimental accuracy with which x is reported in the literature is only about ±1%. Furthermore, because the parameters for band structure calculations are adjusted to reproduce the experimental data for the gaps,² the calculated band structures also have about the same uncertainty. An experimental study is, therefore, necessary to determine which range of alloy compositions have topologically trivial and which have topologically nontrivial L-point bands, irrespective of the presence of a trivial T-point band. He et al.9 describe a method to identify topologically non-trivial properties of the band structure, whereby the Landau level index is plotted vs 1/B. In Weyl semimetals, the plot does not extrapolate to zero, but to a value β that comes from a Berry phase. The problem with this method is that many other factors affect the phase of quantum oscillations: Shoenberg 10 mentions that departures from the LK predictions (about phase) may occur if complications such as spin-dependent impurity scattering or sample inhomogeneity are relevant. Experimentally, it is safer to rely on the period of the oscillations than on their phase. In this article, we describe a method for this condition based on the temperature dependence of the frequency F(T) of SdH oscillations. At T=0, F(T=0) itself is a measure of the cross-sectional area of the Fermi surface $A(E_F) = (e/h) F$ normal to the direction of the applied field [the Fermi energy is $E_F = \mu(T=0)$]. At finite temperature, F(T)probes the cross-sectional area of the Fermi surface $A(\mu, T)$ averaged over an energy range $\sim k_B T$ near μ , as depicted in Fig. 1(b). This potentially contains two mechanisms that give rise to $\frac{dF(T)}{dT} \neq 0$. First, there is a change in $\mu(T)$ with T, called the "Sommerfeld correction." The second mechanism is reported by Guo et al. 22 and is present even when μ is constant (e.g., at E_F). It shown in that publication to be larger than the first in Dirac bands. From Lifshitz-Kosevich theory¹³ combined with Roth's derivation, 14 a Taylor expansion of SdH oscillation frequency as a function of temperature is given by 12

$$F(\mu, T) = F_0(\mu) - \frac{\pi^2}{4} \frac{(k_B T)^2}{\mu_B} \left| \frac{\partial m_c}{\partial E} \right|, \tag{4}$$

where μ_B is the Bohr magneton. At temperatures such that $2\pi^2 k_B T > \hbar \omega_C$, where ω_C is the electron cyclotron frequency, the temperature dependence of the quantum oscillation frequency F(T)is a measure of $-\left|\frac{\partial m_C}{\partial E}\right|$ and the energy derivative of the cyclotron mass m_c . In topologically trivial bands with a parabolic dispersion, the effective mass is constant, which means that $-\left|\frac{\partial m_C}{\partial E}\right|$ is zero. When the dispersion is Dirac-like and given by Eq. (1) (the case depicted in Fig. 1 at the $x = x_c$ range), the effective mass increases as E moves away from the Dirac point $\left(\frac{\partial (\log m_c)}{\partial E} = \frac{1}{|u|}\right)$ and the $-\left|\frac{\partial m_C}{\partial F}\right|$ correction term, which is proportional to v_F^{-1} . What physically happens [see Fig. 1(b)] is that the heavier, higher-energy charge carriers are less likely to complete cyclotron orbits before encountering a phonon that perturbs the phase coherence of their wavefunction shown in Fig. 1(b). The thermal average of the Fermi surface area $A(\mu, T)$ that gives rise to F(T) is thus skewed toward lower-energy electrons in the Fermi distribution; these have a smaller Fermi surface cross section so that the measured quantum oscillation F(T) at finite temperature decreases with increasing T. The experimental test for an alloy composition to have reached $x = x_c$ is, therefore, to observe that $\frac{dF(T)}{dT} < 0$. One does have to verify on a case by case basis that this Dirac term is larger than the Sommerfeld correction,¹¹ which in the semimetallic $Bi_{1-x}Sb_x$ $(x < x_c)$ alloy system is done in the Appendix.

EXPERIMENT

A series of Bi_{1-x}Sb_x samples with nominal concentration of antimony, (x = 2.1%, 3.3%, 4.1%, 5.3%, and 7.2%) were prepared by the traveling molten zone (TMZ) method described elsewhere.² The sample properties are summarized in Table I. The trigonal direction was identified visually and verified by X-ray diffraction (XRD). The nominal antimony concentration was obtained from these XRD spectra at 300 K and comparing the positions of the (009) peaks with the values given by Cucka and Barrett¹⁵ for alloys

TABLE I. Properties of the Bi_{1-x}Sb_x samples studied here. The nominal concentration was obtained from x-ray diffraction and from the position of the (009) peaks. The concentration was double-checked by x-ray fluorescence. The carrier concentration and mobility were obtained from low-field measurements of the Hall coefficient $\rho_{zx}(B_v)$ and resistivity ρ_{zx} . The Shubnikov-de Haas frequency (F) is obtained in $R_{zz}(B_z)$.

Nominal <i>x</i> (XRD, %)	2.1 ± 0.7	3.3 ± 0.7	4.1 ± 0.6	5.3 ± 0.8	7.2 ± 0.6
Concentration x (XRF, %)	1.9 ± 0.3	3.1 ± 0.3	4.6 ± 0.4	5.7 ± 0.4	6.8 ± 0.3
Carrier concentration (cm ⁻³) at 10 K	$8.9 \times 10^{16} (n)$	$8.3 \times 10^{16} (n)$	$4.5 \times 10^{16} (n)$	$1.4 \times 10^{16} (n)$	$3.2 \times 10^{15} (p)$
Mobility (cm ² V ¹ s ⁻¹) at 10 K	1.8×10^{6}	1.9×10^{6}	3.5×10^{6}	1.3×10^{6}	4.9×10^{5}
SdH frequency F (T) at 2 K	4.31 ± 0.35	3.50 ± 0.34	2.47 ± 0.59		
Fermi surface area (m $^{-2}$) normal to the z-axis	$4.11 \pm 0.48 \times 10^{16}$	$3.34 \pm 0.45 \times 10^{16}$	$2.36 \pm 0.70 \times 10^{16}$		•••

in the same composition range. The error bar was obtained by repeating the experiment multiple times and taking the standard deviation around the average value. The main source of error comes from small misalignments of the sample surface vis-à-vis the diffracting surface. The concentration was verified using X-ray fluorescence (XRF) based on the composition of polycrystalline alloys prepared by quenching. Table I shows that the two methods gave consistent results.

The samples were cut into a cuboid shape of approximate dimensions $0.5 \times 0.5 \times 3$ mm for transport measurements, with the sample long dimension along the trigonal (z) axis. Resistivity and Hall effect measurements were made using an AC bridge, Lake Shore 370, in a Quantum Design PPMS system using the AC resistivity/Hall puck, at temperatures from 300 to 2 K and in magnetic fields of up to 7 T.

RESULTS AND DISCUSSION

The convention used here for galvanomagnetic transport measurements of a resistivity labeled $\rho_{ii}(B_k)$ is that the first index (i) is that of the crystallographic direction of the current applied to the sample, the second (j) is the measured electric field, and the third (k) is the direction of the applied magnetic field. Thus, $\rho_{zz}(B_z)$ is the longitudinal magnetoresistance along the trigonal axis, and $\rho_{zx}(B_y)$ is the transverse Hall effect in the bisectrix (y) magnetic field. The temperature dependence of the zero-field trigonal resistivity is shown in Fig. 2(a). The Hall resistivity $\rho_{zx}(B_y)$ at low field (-0.5 to 0.5 T) is shown in Fig. 2(b).

The magnetic-field dependence of the Hall resistivity $\rho_{zx}(B_y)$ is extremely non-linear due to the simultaneous presence of electrons and holes. 16 This electron/hole compensation makes it impossible to derive the properties of the majority carrier from Hall measurements when the field is along the trigonal direction. However, in the low-field limit of $\rho_{zx}(B_v)$, it is possible to derive the carrier concentration and mobility of the carrier with the highest mobility (here the carriers in the L-point bands) from the equations in Ref. 17,

$$n = \lim_{B_y \to 0} \frac{eB_y}{\rho_{zx}(B_y)},$$

$$\mu_m = \lim_{B_y \to 0} \frac{\rho_{zx}(B_y)}{\rho_{zz}(0)},$$
(5)

where μ_m denotes the mobility. These values are shown as a function of temperature in Fig. 3(a). The mobility of all samples reaches several million cm²/V s at 10 K, indicative of the excellent sample quality. The electron concentration in the 5.3% sample and the hole concentration in the 7.2% sample decrease steadily with decreasing T and reach very low values at 10 K (shown in Table I). Since there are about 6×10^{22} atoms/cm³ in Bi, a residual carrier concentration of $3.2 \times 10^{15} \, \text{cm}^{-3}$ in the semiconducting 7.2% alloy indicates that the concentration of residual dopants in these alloys is of the order of 5×10^{-8} atom fraction. With the most common residual impurities in Bi being Pb and Sn, both acceptors, 16 the p-type nature of the 7.2% alloy can be attributed to impurities in the starting materials. The mobility of the 7.2% sample below 30 K decreases with decreasing temperature, indicating ionized impurity scattering, which is also consistent with this hypothesis. The 7.2% ℵ alloy is thus a semiconductor and, at a temperature above 20 K where the charge carrier concentration becomes activated, is an intrinsic semiconductor. In the presence of a magnetic field, it is expected to become an ideal WSM, as did the samples in Ref. 2.



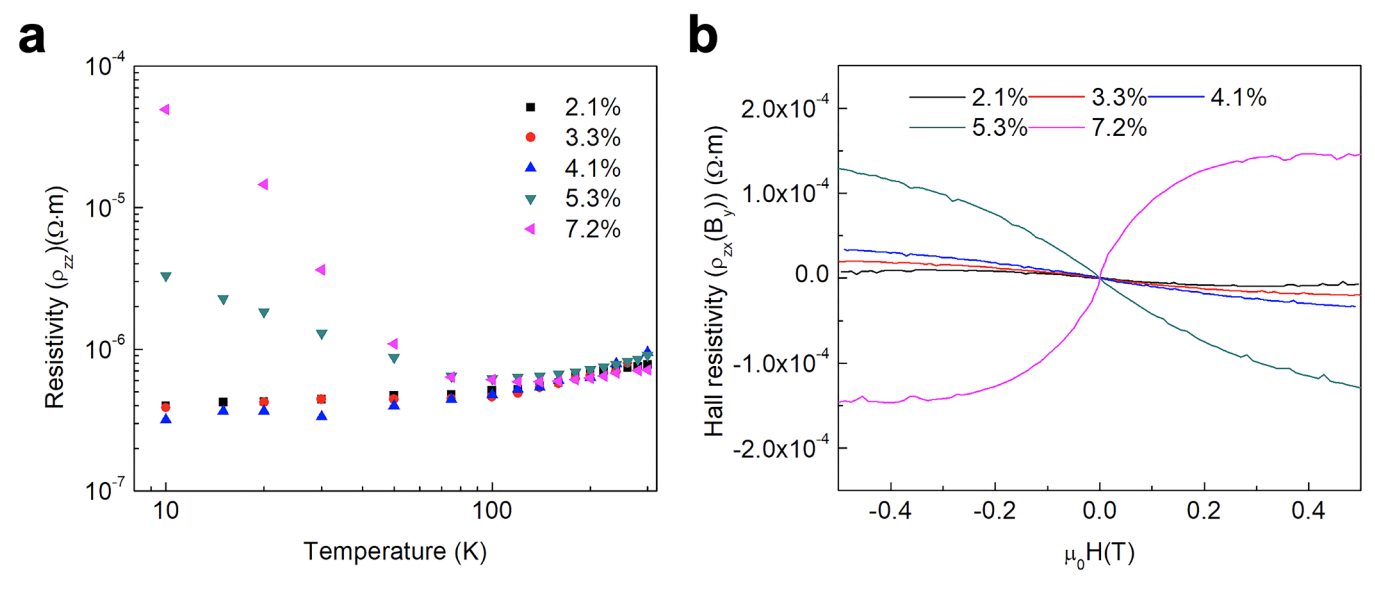


FIG. 2. Temperature dependence of (a) the resistivity at zero magnetic field. (b) The Hall resistivity at 10 K vs magnetic field (b).

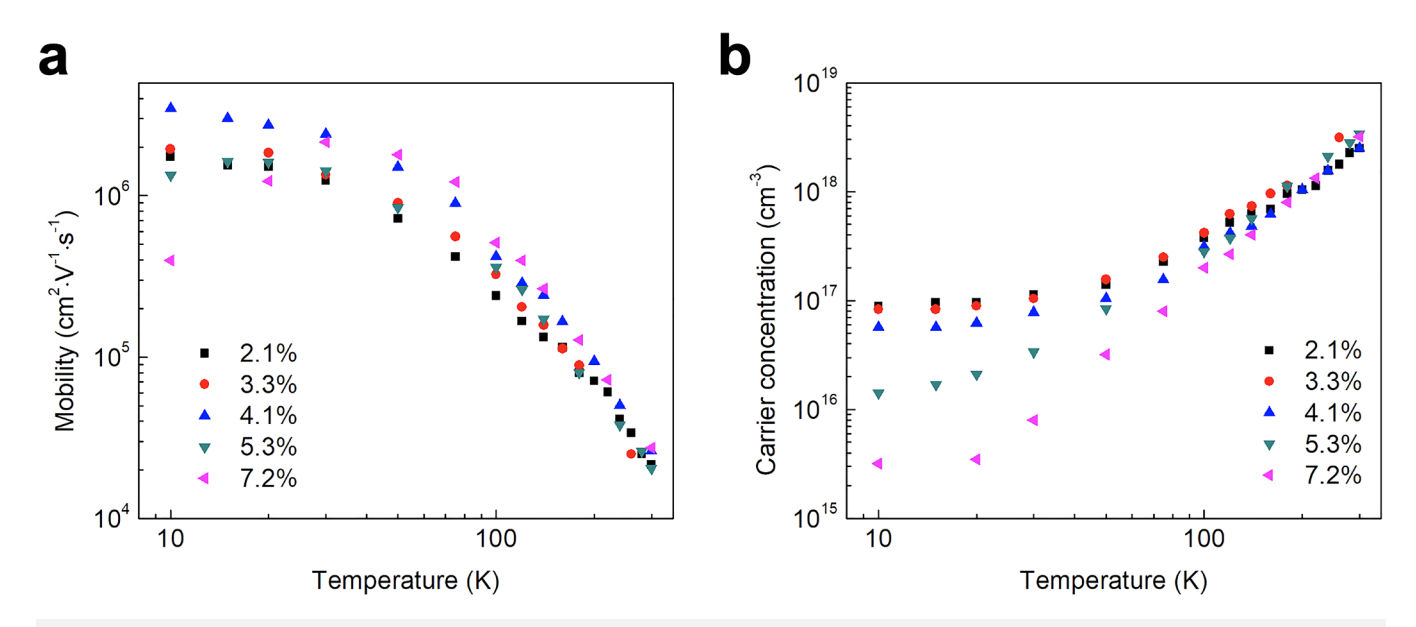


FIG. 3. Temperature dependence of (a) the mobility along the trigonal direction vs temperature. (b) The low-field electron (samples 2.1%-5.3%) or hole (7.2% sample) concentration.

The other alloys are n-type. The 2.1%, 3.3%, and 4.1% alloys' electron concentrations at 10 K are in the high-10¹⁶ cm⁻³ range and temperature independent up to 20-30 K, which is an indication that they are semimetals in which the presence of the T-point band determines the position of μ . This conclusion is again consistent with the observation that their mobility shows no trace of decrease with decreasing temperature, indicating that if ionized impurities are present, their scattering effect is screened by free electrons that do not arise from doping. The charge neutrality condition in semimetals imposes that there are as many electrons as holes within the density of acceptor impurities. Because all samples were prepared from the same starting materials and using the same synthesis procedure, we can assume that this density is of the order of 3×10^{15} cm⁻³ as in the semiconducting 7.2% alloy. In the semimetals, the low-field Hall effect still mostly measures the concentrations of electrons, reported in Table I, because the electron mobility in the L-point conduction bands is much higher than that in the T-point hole band in Bi, 18 a situation that is reasonable to assume that it extends to the semimetallic Bi_{1-x}Sb_x alloys that have similar band structures. The 5.3% sample represents an intermediate case.

The resistance and longitudinal magnetoresistance $R_{zz}(B_z)$ of the samples are reported in Fig. 4 at 2, 3, 5, 10, 15, and 20 K. The 2.1%, 3.3%, and 4.1% samples, which the Hall effect measurements reveal to be semimetals with μ in the L-point valence band, clearly show quantum oscillations at one single frequency, the SdH effect. The background shows a NLMR, but this cannot be taken as being a real physical magnetoresistance because Bi and its alloys are extremely prone to displaying current jetting⁴ and only extraordinary precautions² can avoid this. The behavior of the 5.3% sample is ambiguous, as either the period of oscillations, if they exist, cannot be resolved in the fields available, or the sample reached the

extreme quantum limit (EQL) already at 2 T, as do the semiconducting samples in Ref. 2, or the observed features in the MR are R due to current jetting. The 7.2% sample shows no oscillations at all.

to current jetting. The 7.2% sample shows no oscillations at all. After background subtraction, it is possible to Fourier transform the oscillations' frequency in 1/B and derive a frequency F(x,T) at each concentration and temperature. The values for F(x,T)T = 2 K) are reported in Table I. The corresponding values for $\frac{80}{5}$ the Fermi surface cross section $A(\mu \ T)$ are also reported. In order to establish that the observed oscillations arise from the L-point electrons, and not the T-point holes, the following procedure was developed. In Bi, the T-point hole bands are parabolic and the Fermi surfaces are ellipsoids of revolution with an effective mass along the trigonal axis $m_{T,z} = 0.67$ m_e and masses in the trigonal plane of $m_{T,x} = m_{T,y} = 0.064$ m_e (m_e is the free electron mass). Assuming that the T-hole band masses remain the same in $Bi_{1-x}Sb_x$ for x < 5%, it is thus possible to calculate the hole concentration from the Fermi surface cross section. We obtain for the 2.1% sample $p = 1.6 \times 10^{17} \text{ cm}^{-3}$, for the 3.3% sample $p = 1.2 \times 10^{17} \text{ cm}^{-3}$, and for the 4.1% sample $p = 7.1 \times 10^{16} \text{ cm}^{-3}$ numbers that are clearly not compatible with the densities obtained by the Hall measurements in Table I. The lack of correspondence invalidates the hypothesis that the oscillations are due to T-point holes and thus points to the oscillations being due to electrons at the L point. The L-point bands change strongly from more parabolic to Dirac-like with increasing x so that assuming their constancy with x is not an acceptable hypothesis.

It is now possible to plot the change of F(x,T) as a function of temperature, which is done in Fig. 5. The theoretical prediction 11 that $\frac{dF(T)}{dT} < 0$ in an alloy of composition such that the L-point band has a Dirac dispersion, and not in trivial bands, is strikingly confirmed by the experiment. The Sommerfeld correction to the

2K

FIG. 4. Raw traces of $R_{zz}(B_z)$ in five different concentrations of x showing the Shubnikov-de Haas oscillations. The absolute values of the resistivity are not reliable due to the current-jetting effects contributing to the observed decrease in resistivity with field.

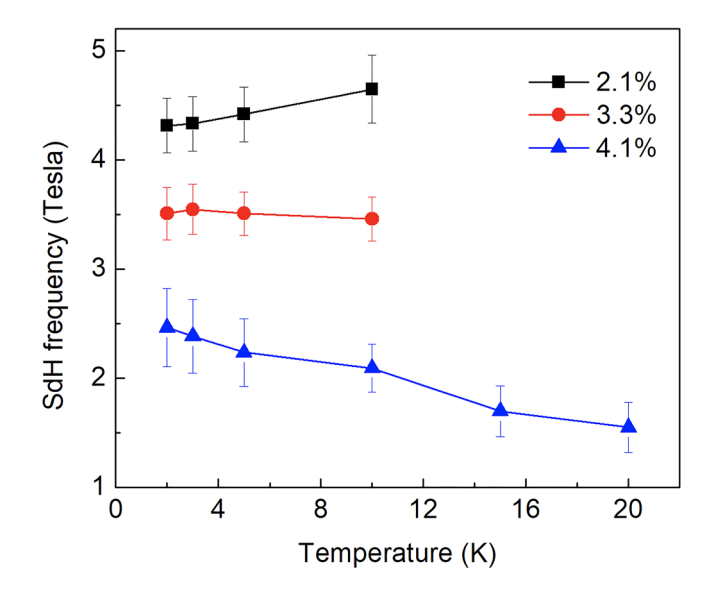


FIG. 5. Temperature dependence of the Shubnikov-de Haas frequency for three different concentrations of x.

SdH frequency is considered and shown in the Appendix to be much smaller than the effect of the Dirac dispersion in the semimetallic Bi-Sb alloys. The error bars were determined from the fullwidth half maximum of the Lorentzian fit made through the 8 Fourier transform of the data. It is also interesting to note that, while the alloys with trivial bands see a decay of this bandwidth, so much that the error bars on the 2.1% and 3.3% samples at 15 and 88 20 K are prohibitively large, the oscillations on the 4.1% sample remain well resolved even at 20 K. We submit that this experiment is another experimental proof of the validity of the theory in $\overset{\hookrightarrow}{\circ}$ Ref. 10 and may even be somewhat more systematic than the proof offered there because the authors in Ref. 10 had to compare data on completely different systems (Cd₃As₂, LaRhIn₅, and Bi₂O₂Se), whereas here, we show the evolution of $\frac{dF(T)}{dT}$ within one system.

CONCLUSIONS

We experimentally show how the temperature dependence of the frequency of quantum oscillations can be used as a diagnostic tool for the Dirac nature of bands. The uncertainty in composition x of $Bi_{1-x}Sb_x$ alloys is of the order of 1%; this makes it difficult to establish from the literature exactly at which composition x_c the bands are Dirac-like, even if the literature reports a value around 5 ± 1 at. %. Therefore, in a systematic study of the thermal chiral anomaly as a function of x, it is necessary to establish x_c experimentally. We prove here that the method of checking for $\frac{dF(T)}{dT} < 0$ is practical and functional.

ACKNOWLEDGMENTS

This work was supported in part (D.V., J.P.H.) by the National Science Foundation (NSF) MRSEC at OSU, entitled the "Center for Emerging Materials" (Grant No. DMR-2011876), and in part (J.S.K.

and J.P.H.) by the MURI entitled "Extraordinary electronic switching of thermal transport" (Grant No. N00014-21-1-2377).

AUTHOR DECLARATIONS

Conflict of Interest

The authors have no conflicts to disclose.

DATA AVAILABILITY

The data that support the findings of this study are available from the corresponding author upon reasonable request.

APPENDIX: THE SOMMERFELD CORRECTION IN SEMIMETALS

The Sommerfeld correction to the SdH frequency quantifies the effect of the shift in the chemical potential of the sample with temperature on the SdH frequency F(T). In semimetals, unlike in metals or degenerately doped semiconductors, the chemical potential μ is set by the local charge neutrality condition that requires that the density of electrons, n, equals the density of holes, p. Expressing the charge carrier densities as a function of integrals over energy of the density of states (D_e and D_h for electrons and holes, respectively), assuming that the bands are parabolic with density of states mass $m^*_{d,e}$ for electrons and $m^*_{d,h}$ for holes, and integrating by parts, we have ¹⁹

$$n(T) = \int_{0}^{\infty} D_{e}(E) f_{0}(E) dE = D_{0,e} \int_{0}^{\infty} \left(-\frac{\partial f_{0}}{\partial E} \right)_{\mu = \mu_{e}} E^{3/2} dE,$$

$$p(T) = \int_{0}^{\infty} D_{h}(E) f_{0}(E) dE = D_{0,h} \int_{0}^{\infty} \left(-\frac{\partial f_{0}}{\partial E} \right)_{\mu = \mu_{h}} E^{3/2} dE,$$

$$D_{0,e} = \frac{2\sqrt{2}}{3} \frac{(m_{d,e}^{*})^{3/2}}{\pi^{2} \hbar^{3}}; D_{0,h} = \frac{2\sqrt{2}}{3} \frac{(m_{d,h}^{*})^{3/2}}{\pi^{2} \hbar^{3}},$$
(A1)

where the integrals are taken from the band extrema to infinity and the electron and hole chemical potential and μ_e and μ_h are defined with respect to those band extrema. The latter condition imposes that their sum equal the band overlap E_o of the semimetal at each temperature,

$$\mu_{\rho}(T) + \mu_{h}(T) = E_{o}. \tag{A2}$$

Using the Sommerfeld–Bethe expansion of the integrals, the charge neutrality condition n(T) = p(T) becomes ¹⁹

$$D_{o,e}(\mu_e(T))^{3/2} \left(1 + \frac{\pi^2}{8} \left(\frac{k_B T}{\mu_e(T)} \right)^2 \right)$$

$$= D_{o,h}(\mu_h(T))^{3/2} \left(1 + \frac{\pi^2}{8} \left(\frac{k_B T}{\mu_h(T)} \right)^2 \right). \tag{A3}$$

The roots of the system of Eqs. (A2) and (A3) can be estimated numerically given that the Fermi energies are known²⁰ for

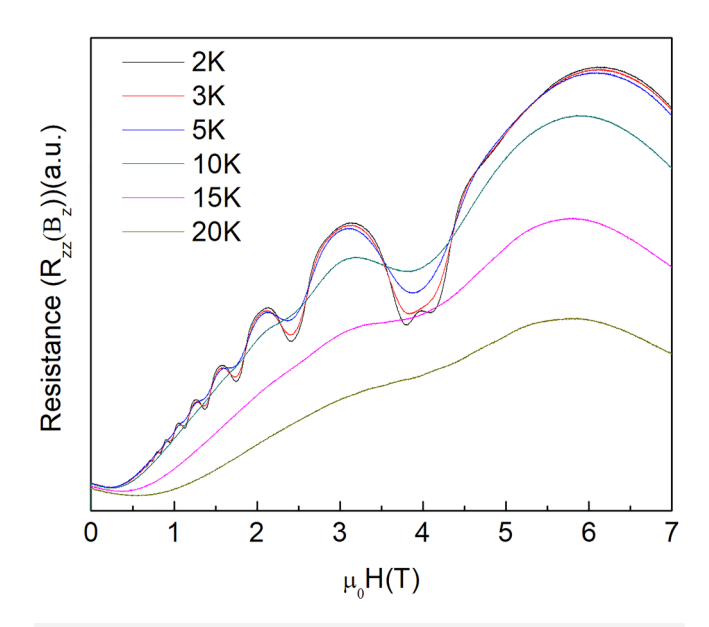


FIG. 6. Raw traces of $R_{\rm zz}(B_{\rm z})$ in bismuth showing the Shubnikov-de Haas oscillations.

elemental Bi to be μ_e $(T=0~{\rm K})=27.2~{\rm meV}$ and μ_h $(T=0~{\rm K})=10.8~{\rm meV}$ and thus, $E_o=38~{\rm meV}$ and the ratio $D_{o,e}/D_{o,h}$ $\stackrel{\rm NS}{=} 0.25$. The result is that μ_e $(T=20~{\rm K})=27.34~{\rm meV}$ and μ_h $\stackrel{\rm NS}{=} 0.25$. The result is that μ_e $(T=20~{\rm K})=27.34~{\rm meV}$ and μ_h $\stackrel{\rm NS}{=} 0.25$. The result is that μ_e $(T=20~{\rm K})=27.34~{\rm meV}$ and μ_h $\stackrel{\rm NS}{=} 0.25$. The result is that μ_e $(T=20~{\rm K})=27.34~{\rm meV}$ and μ_h $\stackrel{\rm NS}{=} 0.25$. The result is that μ_e $(T=20~{\rm K})=27.34~{\rm meV}$ and μ_h $\stackrel{\rm NS}{=} 0.25$. The result is that μ_e $(T=20~{\rm K})=27.34~{\rm meV}$ and μ_h $\stackrel{\rm NS}{=} 0.25$. The result is that μ_e $(T=20~{\rm K})=27.34~{\rm meV}$ and μ_h $\stackrel{\rm NS}{=} 0.25$. The result is that μ_e $(T=20~{\rm K})=27.34~{\rm meV}$ and μ_h $\stackrel{\rm NS}{=} 0.25$. The result is that μ_e $(T=20~{\rm K})=27.34~{\rm meV}$ and μ_h $\stackrel{\rm NS}{=} 0.25$. The result is that μ_e $(T=20~{\rm K})=27.34~{\rm meV}$ and μ_h $\stackrel{\rm NS}{=} 0.25$. The result is that μ_e $(T=20~{\rm K})=27.34~{\rm meV}$ and μ_h $\stackrel{\rm NS}{=} 0.25$. The result is that μ_e $(T=20~{\rm K})=27.34~{\rm meV}$ and μ_h $\stackrel{\rm NS}{=} 0.25$. The result is that μ_e $(T=20~{\rm K})=27.34~{\rm meV}$ and μ_h $\stackrel{\rm NS}{=} 0.25$.

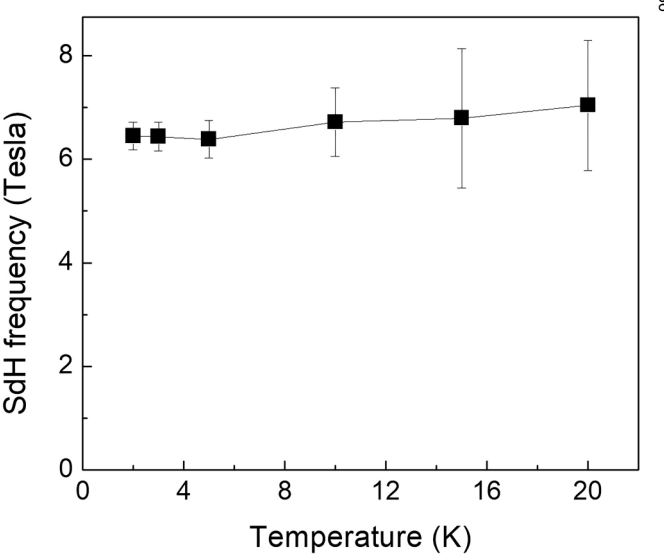


FIG. 7. Temperature dependence of the Shubnikov-de Haas frequency for bismuth.

thus expected to be of the order of a few percent and smaller than the effect of the Dirac bands.

To verify this conclusion experimentally, temperaturedependent Shubnikov-de Haas data were acquired on a single crystal of elemental Bi with the field oriented along the trigonal axis (Fig. 6). These oscillations are due to holes in the parabolic valence band at the T-point of the Brillouin zone. The same data treatment was given; these data were as the ones on the Bi-Sb alloys, and the SdH frequency is given as a function of temperature in Fig. 7. No variation of the frequency can be resolved within the accuracy of the measurement, confirming that the Sommerfeld correction is very small.

REFERENCES

- ¹H. B. Nielsen and M. Ninomiya, "The Adler-Bell-Jackiw anomaly and Weyl fermions in a crystal," Phys. Lett. B 130, 389-396 (1983).
- ²D. Vu, W. Zhang, C. Şahin, M. E. Flatté, N. Trivedi, and J. P. Heremans, "Thermal chiral anomaly in the magnetic-field induced ideal Weyl phase of Bi₁ -rSb₂₂" Nat. Mater. 20, 1525–1531 (2021).
- ³J. Hu, T. F. Rosenbaum, and J. B. Betts, "Current jets, disorder, and linear magnetoresistance in the silver chalcogenides," Phys. Rev. Lett. 95, 186603 (2005).
- ⁴S. Liang, J. Lin, S. Kushwaha, J. Xing, N. Ni, R. J. Cava, and N. P. Ong, "Experimental tests of the chiral anomaly magnetoresistance in the Dirac-Weyl semimetals Na₃Bi and GdPtBi," Phys. Rev. X 8, 031002 (2018).
- ⁵K. Vandaele, M. Otsuka, Y. Hasegawa, and J. P. Heremans, "Confinement effects, surface effects, and transport in Bi and Bi_{1-x}Sb_x semiconducting and semimetallic nanowires," J. Phys.: Condens. Matter 30, 403001 (2018).
- ⁶D. Hsieh, D. Qian, L. Wray, Y. Xia, Y. S. Hor, R. J. Cava, and M. Z. Hasan, "A topological Dirac insulator in a quantum spin Hall phase," Nature 452, 970-974

- C. Şahin and M. E. Flatté, "Tunable giant spin Hall conductivities in a strong spin-orbit semimetal: $Bi_{1-x}Sb_x$," Phys. Rev. Lett. **114**, 107201 (2015). ⁸J. Heremans and J. P. Michenaud, "Electronic magnetostriction of $Bi_{1-x}Sb_x$
- alloys," J. Phys. C: Solid State Phys. 18, 6033-6042 (1985).
- ⁹L. P. He, X. C. Hong, J. K. Dong, J. Pan, Z. Zhang, J. Zhang, and S. Y. Li, "Quantum transport evidence for the three-dimensional Dirac semimetal phase in Cd₃As₂," Phys. Rev. Lett. 113, 246402 (2014).
- 10D. Shoenberg, Magnetic Oscillations in Metal (Cambridge University Press,
- ¹¹N. W. Ashcroft and N. D. Mermin, Solid State Physics (Harcourt College Publishers, 1976).
- 12C. Guo, A. Alexandradinata, C. Putzke, A. Estry, T. Tu, N. Kumar, F.-R. Fan, S. Zhang, Q. Wu, O. V. Yazyev, K. R. Shirer, M. D. Bachmann, H. Peng, E. D. Bauer, F. Ronning, Y. Sun, C. Shekhar, C. Felser, and P. J. W. Moll, "Fingerprint of topology in quantum oscillations at elevated temperatures," arXiv:1910.07608 (2019).
- $^{\bf 13}{\rm I.}$ M. Lifshitz and A. M. Kosevich, "Theory of magnetic susceptibility in metals at low temperatures," Sov. Phys. JETP 2(4), 636-645 (1956).
- 14L. M. Roth, "Semiclassical theory of magnetic energy levels and magnetic susceptibility of Bloch electrons," Phys. Rev. 145, 434-448 (1966).
- 15P. Cucka and C. S. Barrett, "The crystal structure of Bi and of solid solutions of Pb, Sn, Sb and Te in Bi," Acta Crystallogr. 15, 865-872 (1962).
- 16 J.-P. Michenud and J.-P. Issi, "Electron and hole transport in bismuth," Phys. C: Solid State Phys. 5, 3061-3072 (1972).
- ¹⁷J. M. Noothoven van Goor, "Donors and acceptors in bismuth," Philips Res. Rep. Suppl. (4) (1971).
- 18 R. Hartman, "Temperature dependence of the low-field galvanomagnetic coefficients of bismuth," Phys. Rev. 181, 1070-1086 (1969).
- ¹⁹A. Sommerfeld and H. Bethe, Elektronentheorie der Metalle (Springer-Verlag, Heidelberg, 1933), Vol. 24-2, pp. 333-622.
- ²⁰J.-P. Issi, "Low temperature properties of the group V semimetals," Aust. № J. Phys. 32, 585-628 (1979).